THE GAS-ASSISTED FLUID FLOW EXPELLED IN FRONT OF A LONG BUBBLE IN A CIRCULAR TUBE

Cheng-Hsing Hsu[a], Kuang-Yuan Kung[b*], Po-Chuang Chen[a**] and Sam-Dih Huang[a]
[a]Department of Mechanical Engineering
Chung-Yuan Christian University
[b]Department of Mechanical Engineering
Nanya Institute of Technology
414Sec. 3 Chung Shang East R. Chung Li 320
Taiwan, R.O.C.
Contact: ky.kung@msa.hinet.net
**Dr.P.C.Chen works for the Institute of Nuclear Energy Research

Received August 2004, Accepted March 2005
No. 04-CSME-29, E.I.C. Accession 2819

Abstract

This study investigates the steady-state flow field in a circular tube filled with a viscous fluid expelled by a long gas bubble. We use a finite difference method with successive over-relaxation in the computation of the viscous flow field. An empirical bubble profile is employed to simplify the computation of the interface shape between the gas and the viscous fluid. By varying the ratio of the bubble width to the diameter of the circular tube (λ), the numerical simulation shows three fluid flow patterns: the complete bypass flow, the recirculation flow and the transient flow. The transient flow is only observed in a limited λ range of $\sqrt{1/2} < \lambda < 0.7143$ and isn't clearly discussed in the previous studies. The variation of vorticity also is observed by the various sizes of λ.

LE FLUX DE FLUIDE DE GAS-ASSISTED EXPULSÉ DEVANT UNE LONGUE BULLE DANS UN TUBE CIRCULAIRE

Résumé

Cette étude examine le champ d'écoulement à l'état stationaire dans un tube circulaire rempli d'un fluide visqueux expulsé par une longue bulle de gaz. Nous employons une méthode de différence finie avec le sur-relaxation successive au cour du calcul du champ d'écoulement visqueux. Un profil empirique de bulle est utilisé pour simplifier le calcul de la forme d'interface entre le gaz et le fluide visqueux. En changeant le rapport de la largeur de bulle au diamètre du tube circulaire (λ), la simulation numérique donne trois modèles au sujet de l'écoulement de fluide : l'écoulement déviateur complet, l'écoulement de recyclage et l'écoulement transitoire. On n'observe l'écoulement transitoire que dans une gamme limité de λ, soit $\sqrt{1/2} < \lambda < 0.7143$, qui n'était pas clairement discuté dans les études précédentes. On observe également la variation de la vorticité aux tailles diverses de λ.

bubble (half asymptotic bubble width), respectively. The symbols r, z are the cylindrical coordinates. The symbols $\hat{t}$ and $\hat{n}$ indicate the tangential and normal unit vector on the interface. The notations θ, R and λ are defined as the angle between $\hat{n}$ and z axis, the radius of the tube ($R = \overline{BC} = \overline{AF}$), and the ratio of the asymptotic bubble width to the tube diameter (i.e., $\lambda = \overline{EF}/\overline{BC}$), respectively.

The following assumptions are used to simplify the problem.

1. Inviscid driving gas steadily expels the incompressible Newtonian fluid.
2. Neglect the effect of gravity.
3. The axial symmetry condition is considered.
4. The empirical equation of the bubble profile, deduced from Pitts [8] and Hsu and Huang [9], is employed as a known boundary in the computations.
5. The origin of coordinates is located at the bubble's tip.
6. At the far upstream, $z = 3R$ by Cox [7], the flow field fits the Hagen-Poiseuille law.
7. At the far downstream, $z = -3R$ by Cox [6], the contour of bubble is nearly parallel to the channel wall.
8. No-slip condition is used on the tube wall.

Following these assumptions, the continuity equation and the momentum equations of the viscous fluid in the tube are expressed as

$$\frac{1}{r}\frac{\partial(ru_r)}{\partial r} + \frac{\partial u_z}{\partial z} = 0 \tag{1}$$

$$u_r\frac{\partial u_r}{\partial r} + u_z\frac{\partial u_r}{\partial z} = -\frac{1}{\rho}\frac{\partial p}{\partial r} + \upsilon\left(\frac{1}{r}\frac{\partial}{\partial r}\left(r\frac{\partial u_r}{\partial r}\right) + \frac{\partial^2 u_r}{\partial z^2} - \frac{u_r}{r^2}\right) \tag{2a}$$

$$u_r\frac{\partial u_z}{\partial r} + u_z\frac{\partial u_z}{\partial z} = -\frac{1}{\rho}\frac{\partial p}{\partial z} + \upsilon\left(\frac{1}{r}\frac{\partial}{\partial r}\left(r\frac{\partial u_z}{\partial r}\right) + \frac{\partial^2 u_z}{\partial z^2}\right) \tag{2b}$$

The stream function $\psi(r,z)$ and the vorticity ω are define as

$$u_r = -\frac{1}{r}\frac{\partial \psi}{\partial z}, \quad u_z = \frac{1}{r}\frac{\partial \psi}{\partial r} \tag{3}$$

$$\omega = \text{curl}\,\vec{\mathrm{V}} = -\frac{1}{r}\left(\frac{\partial^2\psi}{\partial r^2} + \frac{\partial^2\psi}{\partial z^2} - \frac{1}{r}\frac{\partial \psi}{\partial r}\right) \tag{4}$$

Combining equations (3) and (4) and substituting into (2), then one gets

$$\frac{\partial^2\omega}{\partial r^2} + \frac{1}{r}\frac{\partial\omega}{\partial r} + \frac{\partial^2\omega}{\partial z^2} - \frac{\omega}{r^2} = 0 \tag{5}$$

By introducing the following dimensionless variables

$$r^* = \frac{r}{R},\ z^* = \frac{z}{R},\ u_r^* = \frac{u_r}{U(1-\lambda^2)/2},\ u_z^* = \frac{u_z}{U(1-\lambda^2)/2},\ \omega^* = \frac{\omega}{U(1-\lambda^2)/2R},\ \psi^* = \frac{\psi}{U(1-\lambda^2)R^2/2}$$

where U is the constant velocity of the bubble and equations (5) and (4) can be rewritten as

$$\frac{\partial^2\omega^*}{\partial r^{*2}} + \frac{\partial^2\omega^*}{\partial z^{*2}} + \frac{1}{r^*}\frac{\partial\omega^*}{\partial r^*} - \frac{\omega^*}{r^{*2}} = 0 \tag{6}$$

$$\frac{\partial^2\psi^*}{\partial r^{*2}} + \frac{\partial^2\psi^*}{\partial z^{*2}} - \frac{1}{r^*}\frac{\partial\psi^*}{\partial r^*} + r^*\omega^* = 0 \tag{7}$$

The boundary conditions are derived as follows

(a). From assumption (8), the stream function and the vorticity are

$$\psi^* = -1; \quad \omega^*_{i,j_s} = 2\left[-\frac{1}{(\mathrm{rd})^2} - \frac{1}{(\mathrm{rd})^2}\psi^*\Big|_{i,j_{s-1}} + \frac{2}{1-\lambda^2}\left(\frac{1}{\mathrm{rd}} - \frac{1}{2}\right)\right] \tag{8}$$

where j_s denotes the r-position from the tube wall and rd denotes the grid size on the lower part of the specified location (i, j).

(b). From assumption (6), the far upstream section ($\overline{BC}$) conditions are

$$\psi^* = \frac{\lambda^2}{1-\lambda^2}\left(2r^{*2} - r^{*4}\right) - \frac{r^{*2}}{1-\lambda^2}; \quad \omega^* = \frac{8\lambda^2}{1-\lambda^2}r^* \tag{9}$$

(c). Due to assumption (3), The symmetry conditions at the centerline ($\overline{CD}$) are

$$\psi^* = 0; \quad \omega^* = 0 \tag{10}$$

(d). From assumption (4), an empirical equation of the bubble contour ($\overline{DE}$) is used. No diffusion across the interface and zero tangential stress on the interface of two fluids are imposed as in Cox [6]. Thus, two relative equations at the interface are,

$$u_r^* \sin\theta + u_z^* \cos\theta = 0 \tag{11}$$

$$\left(\frac{\partial u_r^*}{\partial r^*} - \frac{\partial u_z^*}{\partial z^*}\right) 2\sin\theta\cos\theta + \left(\frac{\partial u_r^*}{\partial z^*} + \frac{\partial u_z^*}{\partial r^*}\right)\left(\cos^2\theta - \sin^2\theta\right) = 0 \tag{12}$$

Combining equations (11)-(12) the equation of vorticity on the interface is

$$\omega^* = \frac{2\tan\theta}{r^*}\frac{\partial\psi^*}{\partial x^*}\frac{d\theta}{dx^*} \tag{13}$$

Consequently, the flow conditions on the interface are

$$\psi^* = 0; \quad \omega^* = \frac{2\tan\theta}{r^*}\frac{\partial\psi^*}{\partial x^*}\frac{d\theta}{dx^*} \tag{14}$$

(e). Due to assumption (7), the flow conditions at the far downstream section ($\overline{EA}$) are,

$$\psi^* = \frac{-r^{*2} + \lambda^2}{1-\lambda^2}, \text{ when } \lambda \le r^* \le 1; \quad \omega^* = 0 \tag{15}$$

Note that the boundary conditions at the far upstream and downstream sections will affect the flow fields. The distribution of ψ^* at the far upstream section (Hagen-Poiseuille flow) can be expressed as

$$\psi^* = \frac{\lambda^2}{1-\lambda^2}\left(2r^{*2} - r^{*4}\right) - \frac{r^{*2}}{1-\lambda^2} \tag{16}$$

This equation also indicates that the locations of all the points on that streamline vary as a function of r^* and λ. By setting $\psi^* = 0$ in equation (16), one will get the relative relationship of λ and r^* from the above equation as

$$\lambda = \sqrt{\frac{1}{2 - r^{*2}}} \tag{17}$$

From equations (16) and (17), the location of $\psi^* = 0$ varies as a function of r^* and λ. The position of $\psi^* = 0$ is located on $r^* = 0$, which is the central line, resulting in $\lambda = \sqrt{1/2}$. The value of λ increases from $\sqrt{1/2}$ to 1 when r^* increases from 0 to 1. The critical value $\lambda = \sqrt{1/2}$ will divide the two typical flow patterns, complete bypass flow and recirculation flow, proposed by Taylor [3], Cox [7], Reinelt and Saffman [10], Giavedoni and Saita [17]. In other words, the recirculating flow pattern will be observed if the value of λ is higher than $\sqrt{1/2}$, and bypass flow is seen when $\lambda < \sqrt{1/2}$

3 *Numerical Scheme*

A finite-difference method with Successive Over-Relaxation is used to analyze the present study. The finite difference formulas are derived from equation (6) as

$$\omega_{i,j}^{*K+1} = \frac{\alpha}{e}\left(a\omega_{i+1,j}^{*K} + b\omega_{i,j+1}^{*K} + c\omega_{i-1,j}^{*K+1} + d\omega_{i,j-1}^{*K+1}\right) + (1-\alpha)\omega_{i,j}^{*K} \tag{18}$$

where

$$a = \frac{2}{zr(zr+zl)},\quad b = \frac{2 + rd/r|_j}{ru(ru+rd)},\quad c = \frac{2}{zl(zr+zl)},\quad d = \frac{2 - ru/r|_j}{ru(ru+rd)},\quad e = \frac{2}{zr\times zl} + \frac{2}{ru\times rd} + \frac{zl-zr}{zr\times zl\times r|_j} + \frac{1}{(r|_j)^2}$$

α, K, i, j, zr, zl, ru, rd, denote the over-relaxation factor, iterative time, index at z-direction and r-direction, the grid size on the right side, left side, up side and down side of the specific location (i, j). The difference formula of the stream function for equation (7) is

$$\psi_{i,j}^{*K+1} = \frac{\alpha}{e_1}\left(a_1\psi_{i+1,j}^{*K} + b_1\psi_{i,j+1}^{*K} + c_1\psi_{i-1,j}^{*K+1} + d_1\psi_{i,j-1}^{*K+1} + r|_j\,\omega_{i,j}^{*K+1}\right) + (1-\alpha)\psi_{i,j}^{*K} \tag{19}$$

where

$$a_1 = \frac{2}{zr(zr+zl)},\quad b_1 = \frac{2 - rd/r|_j}{ru(ru+rd)},\quad c_1 = \frac{2}{zl(zr+zl)},\quad d_1 = \frac{2 + ru/r|_j}{ru(ru+rd)},\quad e_1 = \frac{2}{zr\times zl} + \frac{2}{ru\times rd} - \frac{zl-zr}{zr\times zl\times r|_j}$$

The values of ω^* and ψ^* are then calculated from equation (18) and (19) until it reaches the converge criteria

$$\left|\frac{\psi_{i,j}^{*k+1} - \psi_{i,j}^{*k}}{\psi_{i,j}^{*k}}\right| \le 10^{-6} \tag{20}$$

Furthermore, the vorticity on the tube wall can be derived from the wall values of stream function ψ_{i,j_s}^* by using the Taylor expansion. The expansion becomes

$$\psi_{i,j_s-1}^* = \psi_{i,j_s}^* - rd\left.\frac{\partial\psi^*}{\partial r^*}\right|_{i,j_s} + \frac{1}{2}\left.\frac{\partial^2\psi^*}{\partial r^{*2}}\right|_{i,j_s} rd^2 + O(rd^3) \tag{21}$$

Substituting the known value $\psi_{i,j_s}^* = -1$ and rearranging equation (21), the vorticity values on the solid boundary, given in equation (8), can be obtained.

3 *Results and Discussions*

Many previous studies verified two typical flow patterns, the complete bypass flow and the recirculation flow, suggested by Taylor [3]. Cox [7] found the two flow patterns in his experimental work. Reinelt and Saffman [10] verified the two patterns by using the numerical technique. Gauri and Koelling [16] used PTV to measure the velocity and also presented the two patterns. Giavedoni and Saita [17] observed the third pattern which is suggested by Taylor [3], i.e. the stagnation point locates on the centerline between the upstream and the bubble tip. But they didn't have any further discussion or explanation about the phenomenon. Therefore the influence of λ on the streamline and the distribution of vorticity of the flow field is discussed here.

Based upon the study of Pitts [8], the theoretical profile derived agrees well with the experimental results for $\lambda \leq 0.77$. In this study the calculations were performed at values slightly higher than this range to avoid a large deviation from the experimental results.

Figures 2-4 illustrate the three kinds of flow patterns and the distribution of vorticity with the values $\lambda = 0.55$, $\lambda = 0.71$ and $\lambda = 0.8$, respectively. The upper part shows the streamline pattern and the lower part is the vorticity pattern. The streamline in the figures is drawn from $\psi^* = -1$, which is the no slip condition on the tube wall, with the increasing step value 0.1 up to the maximum ψ^* value. The vorticity is drawn with a convenient unit space which depends on the maximum and minimum values, and its value is noted in those figures.

Fig. 2 shows the complete bypass flows. In Fig. 2, the streamlines are seem to be uniform and parallel in the rear region ($-3 \leq z^* \leq -1.8$), and the contour of the bubble is nearly parallel to the tube wall in the far downstream region, as proposed by Cox [6] and Pitts [8]. It shows that the flow velocity in the region is nearly equal and the effect of the vorticity on this region is smaller than on the fluid region of $-1.8 \leq z^* \leq 0$. Also, the effect of vorticity on streamline is trivial in the rear part. Similar parallel phenomenon is found in the far upstream region with uneven streamline spacing. It shows the non-uniform velocity distribution in this region. The streamline deforms largely around the bubble tip region ($-1.0 \leq z^* \leq 1.0$). Consequently, the effects of the vorticity on the flow in this region are higher than the other two. This is especially true in the bubble tip region which contains the region $-1 \leq z^* \leq 1$, where the vorticity values change greatly. In this region, the value changes from ω^*=0.5 to ω^*_{max}=4.0, then it reduce to $\omega^* = 0$ at the tip (0,0). The region where there are large variations in vorticity correspond to regions where the streamline values change quickly. In the region $z^* \geq 0.2$, the value of vorticity increases gradually from ω^*=0 (i.e., at the centerline) to ω^*_{max} in r direction. Thus, the variation of the streamline is dominated by the vorticity value changes in the flow field.

Fig. 3 presents the third flow pattern suggested in Taylor [3] and observed by Giavedoni and Saita [17]. The flow pattern included another zero-value streamline with a stagnation point on the centerline, which results in the third flow pattern as shown. The stagnation point is located at the intersection of the streamline and the centerline. Comparing the streamline patterns of the bypass flow and recirculation flow with those given by Reinelt and Saffman [10], indicate similar flow distributions. It is very interesting to notice that when the λ value is slightly higher than $\sqrt{1/2}$, then the third flow pattern is formed. The recirculation region is formed between the central line and the streamline, including the stagnation point, i.e. $\psi = 0$ in these two lines. In addition, the third flow pattern is the transitional state between the complete bypass flow pattern and recirculation flow pattern, because the phenomenon is shown only near the situation of λ slightly higher than $\sqrt{1/2}$.

Figure 4 shows the typical recirculation flow pattern verified by many previous studies such as Cox [6], Reinelt and Saffman [10], Gauri and Koelling [16] and Giavedoni and Saita [17]. There is a stagnation streamline ($\psi^* = 0$) which starts from the bubble surface and reaches out into the fluid a distance away from the centerline. Between the centerline and the stagnation streamline, the fluid flows in reverse direction away from the bubble. The maximum ψ^* value in this case is higher than zero. This shows the effect of the recirculation flow, and the fluid flows away from it with a slight nip around the nose of the bubble inside this region. Comparing Fig. 3 and Fig. 4, the size of the recirculation zone grows larger and the downstream bypass path of the main flow becomes narrower, when the λ value increases. It is worth noting that the stagnation point moves toward the downstream along the bubble profile and the streamline shows notable change in both the main flow region and the recirculation region when the λ value increases.

From Fig. 2-4, the position of the stagnation point varies with the value of λ. Initially the stagnation point is at the far upstream when $\lambda < \sqrt{1/2}$, while the value of λ increases up to the value of $\sqrt{1/2}$, the stagnation point is on the centerline. It coincides with the bubble tip at $\lambda \approx 0.7143$. In other words, the increment of λ stimulates the movement of the stagnation point from $z^* = 3$ to $z^* = 0$ and is within 0.01 ($\sqrt{1/2} < \lambda < 0.7143$). Thus the transient state is invisible in the previous experimental study. When $\lambda > \sqrt{1/2}$, the stagnation point moves downstream along the bubble profile. In conclusion, the flow pattern first appears as the complete bypass flow, then appears as the transient state flow, and finally appears as the recirculation flow when the λ value increases.

Figure 5 indicates the variation of vorticity on the free surface of the bubble with several different λ values. Values of vorticity in the flow are near zero with any λ at the rear part ($-3 \le z^*$). The maximum value of ω^* changes with λ, and its location drifts away from the bubble tip when λ increases. A noticeable minimum ω^* is also shown with $\lambda > \sqrt{1/2}$. The result also verifies some results of the distribution of the streamline in Fig. 2-4. A negative value of ω^*, which shows the recirculation flow is observed when the λ value is higher than $\sqrt{1/2}$. The location of $\omega^* = 0$ on the bubble surface is the stagnation point and can be found in Fig. 4.

4 Conclusion

The present study numerically employs an empirical equation to analyze the front fluid field of the Newtonian fluid steadily expelled by a long bubble. The study verifies three flow patterns, the complete bypass flow, the transient flow and the recirculation flow. It shows that the third flow pattern, transient flow, is only observed in a limited λ range ($\sqrt{1/2} < \lambda < 0.7143$). The flow pattern first appears as the complete bypass flow ($\lambda \le \sqrt{1/2}$), then the transient state flow ($\sqrt{1/2} < \lambda < 0.7143$) becomes visible, and finally the recirculation flow ($0.7143 \le \lambda$) comes into existence as λ value increases from a lower value to a higher one.

The distribution of vorticity is also shown in the study; it affects the distribution of the streamline in the flow field. As the λ value increases, the location of maximum ω^* value drifts away from the bubble tip, and negative values of maximum ω^* evidently show the recirculation flow when $\lambda > \sqrt{1/2}$.

Acknowledgements

The present work was conducted under support (NSC 94-2212-E-033-018) from the National Science Council, Taiwan, R.O.C.

References:

[1] Fairbrother, F.P. and Stubbs, A.E., Studies in electroendosmosis. Part VI. The bubble tube method of measurement, *J. Chem. Sci.*, Vol. 1, 1935, pp. 527-529.

[2] Saffman, P. G. and Geoffrey Taylor, F.R.S., The penetration of a fluid into a porous medium or Hele-Shaw cell containing a more viscous Liquid, Proc. Roy. Soc A, Vol. 245, 1958, pp. 312-329.

[3] Taylor, G.I., Deposition of a viscous fluid on the wall of a tube, J. Fluid Mech., Vol. 10, 1961, pp. 161-165.

[4] Bretherton, F.P., The motion of long bubbles in tubes, J. Fluid Mech., Vol. 10, 1961, pp. 166-188.

[5] Goldsmith, H.L. and Mason, S.G., The movement of single large bubbles in closed vertical tubes, J. Fluid Mech., Vol. 14, 1962, pp. 42-58.

[6] Cox, B.G., On driving a viscous fluid out of a tube, J. Fluid Mech., Vol. 14, 1962, pp. 81-96.

[7] Cox, B.G., An experimental investigation of the streamlines in viscous fluids expelled from a tube, J. Fluid Mech., Vol. 20, 1964, pp. 193-200.
[8] Pitts, E., Penetration of gluid into a Hele-Shaw cell: The Saffman-Taylor experiment, J. Fluid Mech., Vol. 97, 1980, pp. 53-64.
[9] C. H. Hsu and S. D. Huang, A Flow Visualization of a Long Bubble in a Tube, The Third Pacific Symposium on Flow Visualization and Image Processing, 2001.
[10] Reinelt, D. A. and Saffman, P. G., The penetration of a finger into a viscous fluid in a channel and tube, SIAM J. Sci. Stat. Comput., Vol. 6, 1985, pp. 542-561.
[11] Shen, E. I. and Udell, K. S. A finite element study of low Reynolds number two-phase flow in cylindrical tubes, Trans. ASME, J. Appl. Mech., Vol. 52, 1985, pp. 253-256.
[12] Mavridis, H. and Hrymak, A. N. and Vlachopoulos, J., Finite element simulation of fountain flow in injection molding, Polym. Eng. Sci., Vol. 26, 1986, pp. 449-454.
[13] Schwartz, L.W., Princen, H.M. and Kiss, A.D., On the motion of bubbles in capillary tubes, J. Fluid Mech., Vol. 172, 1986, pp. 259-275.
[14] Poslinski, A.J. and Stokes, V.K., Gas-assisted displacement of a viscous liquid in tube. ANTEC, 1993, pp.68-73.
[15] Huzyak, P.C. and Koelling, K.W., The penetration of a long bubble through a viscoelastic fluid in a tube, J. Non-Newton. Fluid Mech., Vol. 71,1997, pp. 73-88
[16] Gauri, V., Koelling, K. W., Gas-assisted displacement of viscoelastic fluids: flow dynamic at the bubble front, J. Non-Newton. Fluid Mech., Vol. 83, 1999, pp. 183-203.
[17] Giavedoni, M. D. and Saita, F. A., The axisymmetric and plane cases of a gas phase steadily displacing a Newtonian liquid: A simultaneous solution of the governing equations, Phys. Fluids, Vol. 9, 1997, pp. 2420-2428.
[18] Giavedoni, M. D. and Saita, F. A., The rear meniscus of a long bubble steadily displacing a Newtonian liquid in a capillary tube, Phys. Fluids, Vol. 11, 1999, pp. 786-794.
[19] Kamişli, F and Michael E. Ryan, Perturbation method in gas –assisted power-law fluid displacement in a circular tube and a rectangular channel, Chem. Eng. J., 75 (1999) 167-176.
[20] Kamişli, F and Michael E. Ryan, Gas-assisted non-Newtonian fluid displacement in a circular tubes and noncircular channels, Chem. Eng. Sci. , 56 (2001) 4913-4928.
[21] Kamişli, F and Michael E. Ryan, Gas-assisted displacement of a Newtonian fluid confined in a Hele-Shaw cell, Chem. Eng. J., 84 (2001) 193-200.
[22] Kamişli, F., Flow of a long bubble in a square capillary, Chem. Eng. Process. 42 (2003) 351-363.

Nomenclature

R Radius of the tube
U The constant velocity of the bubble
$\overline{V}$ Velocity
m Fractional converge
n The normal unit vector on the bubble interface
p Pressure in the fluid expelled by bubble
r The radial direction in coordinate system
t The tangential unit vector on the bubble interface
u The velocity of the fluid expelled by bubble
z The axial direction in coordinate system

Greek letters

α The over-relaxation factor
θ The angle between the normal of the interface and the axial direction
λ The ratio of the asymptotic bubble width to the inner diameter of the tube

υ Kinematic viscosity
ψ Stream function
ω Vorticity

Superscript
K Iterative time
$*$ Dimensionless form

Subscript
r The radial direction in coordinate system
s Tube wall
z The axial direction in coordinate system

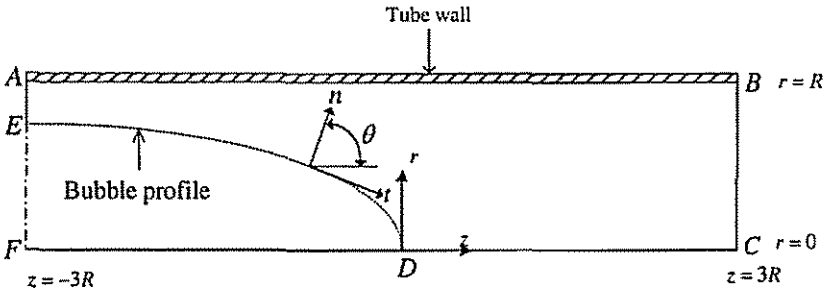

Fig. 1 Physical diagram showing the coordinate system used in the study of a gas bubble steadily expelling viscous fluid.

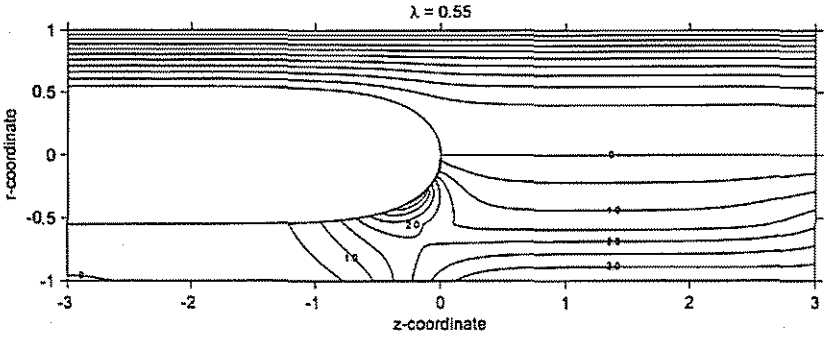

Fig. 2 Distribution of streamline and vorticity for $\lambda = 0.55$

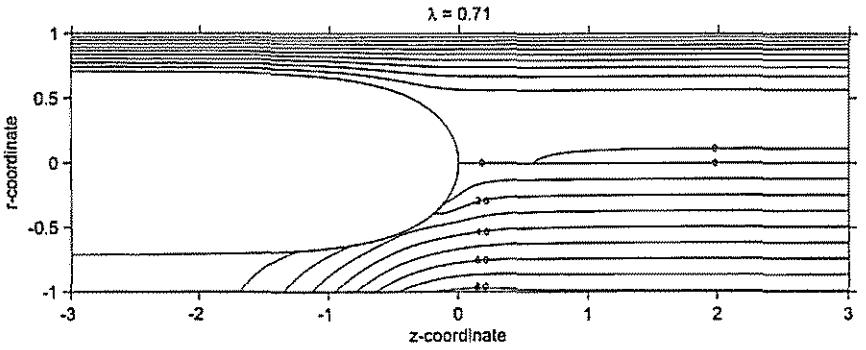

Fig. 3 Distribution of streamline and vorticity for $\lambda = 0.71$

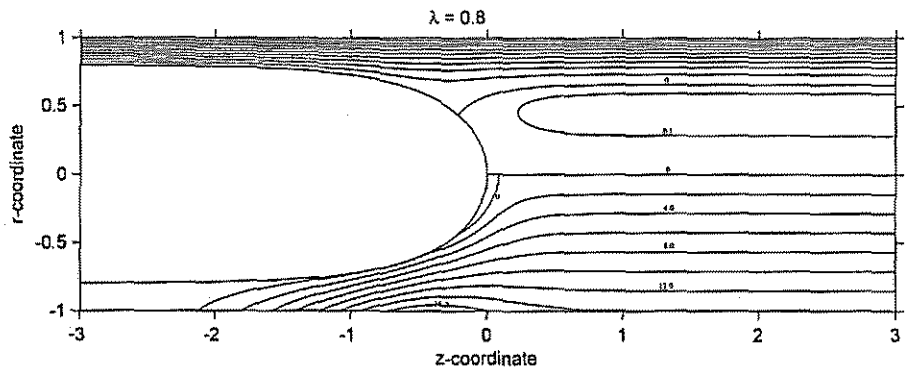

Fig. 4 Distribution of streamline and vorticity for $\lambda = 0.8$

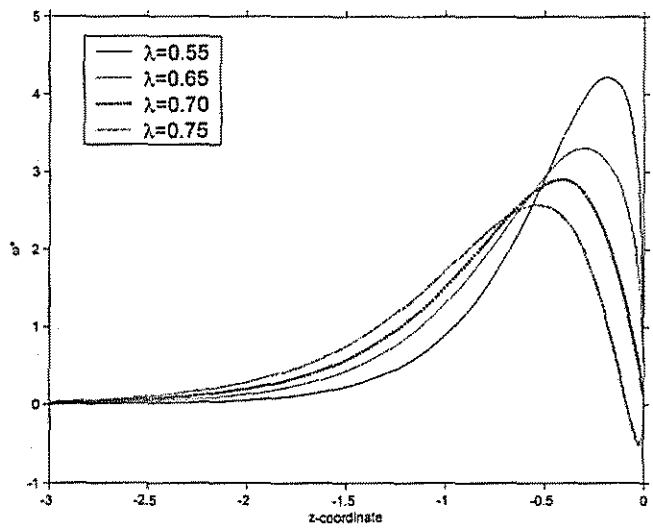

Fig. 5 Distribution of vorticity on the free surface of bubble with different λ values.